# Line-Of-Sight Massive MIMO Channel Characteristics in an Indoor Scenario at 94 GHz

**Article** *in* IEEE Access · October 2018

DOI: 10.1109/ACCESS.2018.2876225

CITATIONS
5

READS
228

**5 authors**, including:

Frédéric Challita
Nokia Bell Labs
**13** PUBLICATIONS **15** CITATIONS
SEE PROFILE

Jose-Maria Molina-Garcia-Pardo
Universidad Politécnica de Cartagena
**180** PUBLICATIONS **1,028** CITATIONS
SEE PROFILE

Davy P. Gaillot
University of Lille Nord de France
**117** PUBLICATIONS **984** CITATIONS
SEE PROFILE

# Line-Of-Sight Massive MIMO Channel Characteristics in an Indoor Scenario at 94 GHz

Frédéric Challita, Maria-Teresa Martinez-Ingles, Martine Liénard, Jose-Maria Molina-Garcia-Pardo, Davy P. Gaillot

***Abstract*—The fading and correlation characteristics of virtual, yet realistic, Line-of-Sight (LOS) 4 $\times$ 2500 millimetric (mmW) massive MIMO channels are investigated at 94 GHz in an indoor office environment for three different Tx-Rx distance scenarios. The capability of the mmW massive MIMO channel to spatially decorrelate the users is evaluated with the computation of the channel correlation and other channel metrics such as power to interference ratio and condition number. In particular, the correlation between channel vectors for a given user and its influence on receiving correlation is discussed. The results clearly demonstrate the capability of mmW massive MIMO systems to reach orthogonal Tx-Rx streams even for a small 7 $\times$ 7 antenna array subset with correlation between users $<$0.2. Moreover, strong phase variations at Tx side at this frequency range are highlighted through channel phase correlation studies and were shown to contribute to the decorrelation at Rx side between close users paving the way for further massive MIMO system enhancements.**

***Index Terms*—Millimeter wave, massive MIMO, indoor propagation.**

## I. Introduction

Global mobile data traffic is expected to grow at a compound annual rate (CAGR) of 47 percent from 2016 to 2021 thus reaching 49 exabytes per month by 2021 [1]. This huge data revolution requires the intensive use of telecom networks and has prompted the research community to develop, among other solutions, MIMO systems in adjunction with the large bandwidth available in the mmW frequency bands.

The mmW technology offers several major benefits. It can be used for high data transmission using low order modulation resulting in less power, reduced complexity, and lower cost. In addition, higher frequencies imply smaller antennas and arrays which could fit into user terminals or adequate for small cells. On the other hand, mmW frequencies are subject to additional isotropic free-space attenuation [2] as well as potential losses due to blockages and specific gases in the environment [3]. Nonetheless, this approach is gaining a lot of momentum in the wireless industry and is on the research agenda of the 2020 5G-PPP initiative [4]. For instance, use-cases and applications such as smart offices, tactile internet, high definition video streaming, automotive radar, security screening, substance identification and non-destructive testing and remote surgery among others are also listed in the mmMAGIC project [5], in [6], [7], [8] and in the European Telecommunications Standards Institute (ETSI) [9].

In parallel, massive MIMO systems, also called very large multi-user (MU)-MIMO, are strongly envisioned to increase the sum rate capacity and energy efficiency. The concept was first introduced in [10] where the author stated that as the number of antennas of the base station (BS) approaches infinity, individual user channels become spatially decorrelated and pairwise orthogonal thus boosting the principle of simultaneous transmissions. It was also shown this approach enables simple linear precoding schemes at low frequency bands [11]. An overview of benefits, opportunities and challenges which flow from Massive MIMO are presented in [12], [13], [14]. However, large-scale MIMO has only been tested in labs [15], [16], [17], [18] and a few field trials [19].

From this discussion, it can be assumed that the association of the massive channel with mmW technology is well suited for 5G systems [20], [21] to improve throughput performance and wireless access. Surveys on mmW massive MIMO communication for future wireless systems are presented in [22], [23], [24]. However, measurements, simulations and performance evaluation of the mmW Massive MIMO channel are scarce (found in [25], [26]). In [27], mmW massive MIMO channel measurements at 11, 16, 28, and 38-GHz bands were conducted in indoor environments. Massive MIMO measurements at 44 GHz with a 48-element active phased-array were performed in [28]. Indoor massive MIMO channel measurements at 13-17 GHz using a vector network analyzer (VNA) and a 20$\times$20-element virtual uniform rectangular array were also reported in [29]. These analysis and measurements are not sufficient to characterize the mmW massive MIMO channel and a thorough analysis and understanding of the indoor massive channel in the mmW band is clearly missing through a depiction of the propagation mechanisms and related parameters retrieved from the measurements.

This work falls within this context and aims at experimentally evaluating the mmW massive MIMO approach in LOS conditions for indoor applications. The massive MIMO radio channel was measured at 94 GHz from the same setup reported in a previous work [30] since this frequency band is yet to be fully addressed in the literature. For instance, the extension of the wireless communications systems to frequencies above 60 GHz (between 60 and 300 GHz) is envisaged by the first phase the EU's Horizon 2020 research program to fill the gap between the millimeter-wave and the terahertz spectrum [5].

This contribution is a preliminary attempt to understand and

F. Challita, D. P. Gaillot, and M. Liénard are with the University of Lille, IEMN, Bâtiment P3,Villeneuve d'Ascq, 59655 FR e-mail: davy.gaillot@univ-lille.fr.

M-T. Martinez-Ingles is with the University Center of Defense, San Javier, Air Force Base, Ministerio de Defensa, UPCT

J-M. Molina-Garcia-Pardo is with the Dpto. Tecnologías de la Información y las Communicaciones, Universidad Politécnica de Cartagena, Cartagena, Spain.

Manuscript received September 19, 2018; accepted October 10, 2018.

quantify the decorrelation mechanisms between users and their origin for this band. Nonetheless, the proposed methodology is applicable to any lower mmW frequencies. For instance, the fading characteristics and channel correlation mechanisms at both the transmitter and receiver side are investigated. In particular, the optimal number of Tx antennas capable of spatially separating a given number of users in the studied indoor environment (can be extended to other environments) is addressed.

The rest of the paper is organized as follows. The channel parameters of interest for a massive MIMO analysis are outlined in section II with a focus on the correlation notion and evaluation metrics. Section III shows the scenario and measurement setup. Before concluding, the different results are presented in Section IV.

## II. Propagation characteristics, channel correlation, evaluation and metrics

Typically, the measured massive MIMO transfer function is given by $\mathbf{H} \in \mathbb{C}^{K\times M\times M_f}$ where $K$, $M$, and $M_f$ are the number of users, transmitting antennas (with $M \gg K$), and frequency points, respectively. Each element $h_{kmf}$ of $\mathbf{H}$ is the extracted complex channel coefficient associating the $k^{th}$ receiver with the $m^{th}$ transmitter at each frequency point $f$. The $k^{th}$ receiver is equipped with a single antenna making the scenario similar to a multi-user MISO setup.

### A. Propagation Characteristics

In general, if the channel vectors to different users are correlated, the benefits of large array systems fade. If the channels exhibit a Rician fading distribution with a dominant LOS component, the contribution of the multipath components (MPC) to the radio channel is reduced as well as the degrees of freedom. The LOS component will exhibit the largest singular value thus absorbing all the energy to the corresponding mobile station in the case of power allocation through waterfilling. Hence, it could be believed that such channels are not favorable in general for massive MIMO for any frequency band. In contrast, the main advantages of massive MIMO are expected when the propagation characteristics are rich (i.e. high degree of freedom). For this case, users can be spatially separated thus enabling the use of linear receiver techniques for uplink and downlink. For instance, Rayleigh fading models provide a much richer environment with a high degree of freedom and would, therefore, display favorable propagation conditions. From this point of view, the Rice factor $K$, defined as the ratio between the LOS and MPC (without the LOS component) power (Eq. (1)) is particularly relevant and critical to describe the complexity of the radio channel for massive MIMO applications and is a preliminary step to investigate the correlation mechanisms discussed in the following sections.

$$K(\text{dB}) = 10\log_{10}\left(\frac{P_{LOS}}{\sum_{i=1}^{N} P_{NLOS}^{i}}\right), \tag{1}$$

where $P_{LOS}$ is the LOS power, $P_{NLOS}^{i}$ is the $i^{th}$ power of the NLOS MPC, and N the number of computed NLOS MPC (or channel taps).

### B. Correlation

The correlation characteristics of the massive MIMO channel $\mathbf{H}$ are split into an analysis of the Rx inter-user correlation and Tx correlation per user. The former and latter are denoted ***Intercorrelation*** and ***Intracorrelation*** throughout the manuscript, respectively.

*1) **Intracorrelation or Tx spatial correlation per user**:* This type of correlation shows the dependence between the channel coefficients for each user and provides additional information about the fading characteristics and any other propagation factors that could participate to the decorrelation of the massive MIMO channel from the Tx side. The intracorrelation $\rho_{km_{ref}}^{intra}$ provides the correlation between the $m_{ref}^{th}$ element of the transmitting array arbitrarily selected as a reference antenna with all the remaining elements $m$ for user $k$ and $M_f$ frequency points:

$$\rho_{km_{ref}}^{intra}(m) = \frac{|\sum_{f=1}^{M_f} h_{km_{ref}f}.h_{kmf}^{*}|}{\sqrt[2]{\sum_{f=1}^{M_f}|h_{km_{ref}f}|^2.\sum_{f=1}^{M_f}|h_{kmf}|^2}}, \tag{2}$$

where $(.)^*$ denotes the complex conjugate. If a single user and one antenna reference are considered, Eq. (2) yields an $M$-element vector by sweeping all the antennas of the array. Generalizing for all users and reference antennas, a $K \times M \times M$ matrix is obtained.

*2) **Intercorrelation or Rx spatial correlation**:* Intercorrelation is the main metric to assess the performance of the massive MIMO system because it helps to predict the precoding matrix and its complexity as well as many signal processing techniques. It provides a better understanding of the system capacity to simultaneously serve a number of users. Intercorrelation can be expressed in a general form as in [31]:

$$\rho_{Rx} = \mathbb{E}\{\mathbf{H}\mathbf{H}^{H}\}, \tag{3}$$

followed by a normalization. In our study, after reshaping $\mathbf{H}$ into a $K \times M \times M_f$ matrix, the $\mathbf{H}.\mathbf{H}^{H}$ (the Gram or inner product matrix for each frequency point where $(.)^{H}$ denotes the Hermitian transpose) product will yield a $K \times K$ matrix which, without normalization, is a measure of the correlation between users. Hence, for any two users $i$ and $j$, the intercorrelation $\rho_{ij}^{inter}$ as a function of the number of antennas selected in the array $M_t$ ($1 \leq M_t \leq M$) is given by:

$$\rho_{ij}^{inter}(M_t) = \frac{1}{M_f}\left(\frac{\sum_{f=1}^{M_f}\sum_{m=1}^{M_t}|h_{imf}.h_{jmf}^{*}|}{\sqrt[2]{\sum_{f=1}^{M_f}\sum_{m=1}^{M_t}|h_{imf}|^2.\sum_{m=1}^{M_t}|h_{jmf}|^2}}\right). \tag{4}$$

*3) Evaluation metrics:*

- *Power to interference ratio*

Although the intercorrelation coefficient is a good indicator of the channel orthogonality between users as the number of emitting antennas is increased, other metrics have also been proposed. As an example, *the power to interference ratio* defined as the diagonal element power of $G$ with respect to the total power per user can be used to evaluate the focusing of

electromagnetic fields [32]. This criterion evaluates how much the other users are affecting the variance or the power intended to a given user. The power to interference ratio $\gamma(\mathbf{G})$ can be formulated as follows:

$$\gamma(\mathbf{G}) = \frac{1}{K}\sum_{i=1}^{K}\gamma_i(\mathbf{G}) = \frac{1}{K}\sum_{i=1}^{K}\left(\frac{|g_{ii}|^2}{\sum_{j=1}^{K}|g_{ij}|^2}\right), \quad (5)$$

where $g_{ij}$ are the elements of $\mathbf{G} = \mathbf{H}.\mathbf{H}^H$ and $\gamma_i(\mathbf{G})$ is the $i^{th}$ element of the $K$-element power to interference ratio vector. In addition, $\gamma(\mathbf{G})$ is an indicator of the percentage of transmitted power to the intended user instead of interfering with other users. Hence, values close to one are desired.

- *Condition number*

Another approach classifying the spatial separation between users is given by *the condition number* of the Gram matrix which here is defined as follows:

$$\kappa = \sqrt{\frac{max(\boldsymbol{\sigma})}{min(\boldsymbol{\sigma})}}, \quad (6)$$

where $\boldsymbol{\sigma} = [\sigma_1, \sigma_2, ..., \sigma_{min(K,M)}]$ are the eigenvalues after the decomposition of the Gram matrix:

$$\mathbf{G} = \mathbf{U}.\mathbf{S}.\mathbf{V}^H, \quad (7)$$

with $\mathbf{U} \in \mathbb{C}^{K\times K}$ , $\mathbf{V} \in \mathbb{C}^{M\times M}$, and $\mathbf{S} \in \mathbb{C}^{K\times M}$. Note that $\kappa$ could also be computed from the SVD (singular value decomposition) of $\mathbf{H}$ but at the expense of increased computational complexity, especially when dealing with large channel matrices. The condition number provides a quantitative criterion on the effectiveness and influence of the possible use of the waterfilling algorithm in the case of optimal power allocation for maximum capacity rate. The condition number is a complementary notion to the SVD spread used to evaluate the joint orthogonality of the user channel vector in a MIMO system. The closer to one is the condition number, the easier it is to separate users thus ensuring orthogonality.

- *Reference scenario*

In order to evaluate the correlation characteristics of the massive array, it is good practice to compare with the classical Rayleigh channel with double-entry independent and identically distributed (i.i.d.) channel coefficients. This is the best case scenario and implemented through a random channel with a large number of observations $N$. The channel matrix model $\mathbf{H} \in \mathbb{C}^{K\times MN}$ is taken as follows:

$$\mathbf{H_{ij}} = \frac{1}{\sqrt{2}}.(\mathbf{H}_{\mathcal{R}} + \jmath\mathbf{H}_{\mathcal{I}}), \quad (8)$$

where $\mathbf{H}_{\mathcal{R}}$ and $\mathbf{H}_{\mathcal{I}}$ are drawn from the normal distribution $\mathcal{N}_c(0, \mathcal{I})$ and are of size $K \times MN$. $N$ is the total number of observations or frequency points.

## III. Measurements: Radio Channel Sounder and Scenarios

The indoor scenario shown in Fig.1 is located in one of the UPCT laboratories, Spain. The dimensions of the room are 8×4.8×3.5 meters (W x L x h) and is furnished with closets, chairs, desktops and shelves. Channel sounding is the process of evaluating the radio propagation environment between any transmitter and receiver. This information is essential for developing robust and reliable wireless systems to transmit data over the radio channel. The mmW channel sounder consists in a RS ZVA-67 VNA and RS ZVA-Z110E up-converters (W-band WR-10, 75 to 110 GHz). The channel transfer functions were obtained via the $S_{21}$ scattering parameter and the system was through calibrated such that the delay and antenna gains are included in the measurements and the effects of the system mitigated. More details on the channel sounding aspects can be found in [30]. The frequency parameters are shown in Table I below:

Fig. 1. Panoramic view of the indoor scenario.

TABLE I
MMW Radio channel sounder configuration

| | |
|---|---|
| Frequency | 94 GHz |
| Span BW | 3 GHz |
| Resolution | 0.33 ns |
| Lower and Upper frequency | 92.5 and 95.5 GHz |
| IF (Intermediate frequency) | 100 Hz |
| Frequency points | 1024 |
| Frequency spacing | 2.932 MHz |
| Dynamic Range | $>$ 100 dB |

A 4-element virtual Uniform Linear Array (ULA) was used for Rx and a massive 50×50 virtual Uniform Rectangular Array (URA) for Tx. The receive antenna has a 0.784 m height while the transmit antenna is 0.886 m above the ground. Identical polarimetric omnidirectional antennas manufactured by Mi-Wave (WR-10) were used [33]. These antennas operate at 94 GHz with 3 GHz bandwidth, 30 degrees beamwidth in elevation and omnidirectional in the horizontal plane, 2 dBi gain and typical nominal VSWR of 1.5:1. Hence, the measured massive MIMO channel $\mathbf{H}$ is of size 4×50×50×1024 (or 4×2500×1024 if reshaped). The Tx and Rx antennas were operated with Arricks Robotics positioners at both sides [34]. The Rx inter-element separation is $d_{Rx} = 100$ mm and the Tx separation is $d_{Tx} = 9.18$ mm corresponding to $\sim 31\lambda$ and $\sim 3\lambda$, respectively, where $\lambda \approx 3.19$ mm is the wavelength at 94 GHz. Hence, the transmitting array spans an area of $150\lambda \times 150\lambda$ ($\sim$ 50 cm × 50 cm). The inter-element spacing at Tx side was selected as a tradeoff between the maximum displacement offered by the positioning system (including coaxial cables for the up-converters) and the achievement of a realistic massive MIMO configuration in this frequency range. For instance, the inter-element spacing was chosen for the ULA (as if we had a real ULA) in order to obtain spatially uncorrelated, yet physically close, Rx users ($d_{Rx} \gg \lambda$). For the URA, the spacing was chosen to obtain mutually

uncoupled Tx antennas as if an equivalent real array was used ($d_{Tx} > \lambda$).

In our study, three URA-ULA positions with increasing Tx-Rx distances were considered for the evaluation of the channel: Close ($d_{Tx-Rx} =$ 2.63 m), center ($d_{Tx-Rx} =$ 4.06 m) and far ($d_{Tx-Rx} =$ 6.02 m). It should be noted that the slightest move strongly modifies the channel in this frequency range and thus longer distances were not required for this study. The measurement was performed under static conditions with no people in the room. These scenarios are illustrated in Fig. 2.

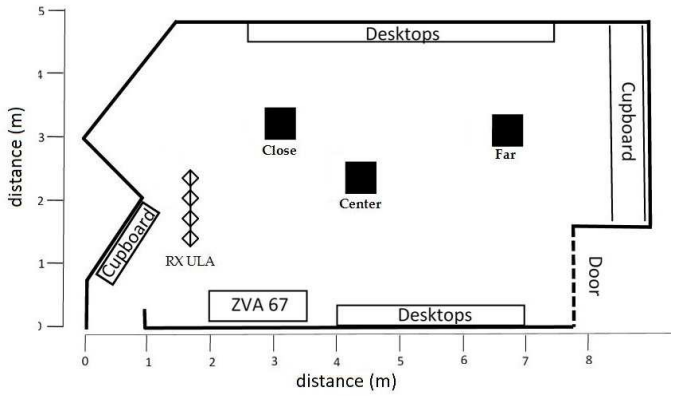


Fig. 2. Top view of the indoor scenario. The three investigated scenarios are labeled as Close, Center, and Far, corresponding to a categorization of the Tx-Rx distance.

## IV. Results and Discussion

First, Fig. 3 presents the Power Delay Profile (PDP) for all Rx users with the Far scenario as an example. The PDP is obtained as the expectation of the inverse Fourier Transform applied to all complex transfer functions and averaged over all Tx antennas. It can be observed numerous MPC for which the delay positions and relative gains nearly correspond between the different users with some differences. For this scenario, the first component (LOS) and the last component contributing to the overall channel energy are separated by nearly 35 ns (distance difference of $\sim$10.5 meters). This shows that the dynamic range of the system is sufficient to collect high-order MPC contributing to the radio channel even in this frequency range.

Nonetheless, this result is misleading because the averaging process is performed over antennas spanning a wide surface area compared to $\lambda$ such that spatial stationarity is not fulfilled. Hence, geometrical parameters can not be estimated with high-resolution estimators like SAGE [35] or RiMAX [36]. It follows each Tx-Rx link must be individually investigated to extract meaningful parameters in the context of massive MIMO. For instance, it is interesting to assess the distribution of the Rice factor $K$, but the number of MPC $N$ observed in the radio channel must be evaluated prior Eq. (1). A specular propagation path is defined as a distinguishable peak in the PDP between the Tx and the Rx. The analysis is performed by counting all identified MPC (LOS and NLOS) within a certain threshold with respect to the maximum gain of the PDP (i.e. LOS). The empirical cumulative distribution

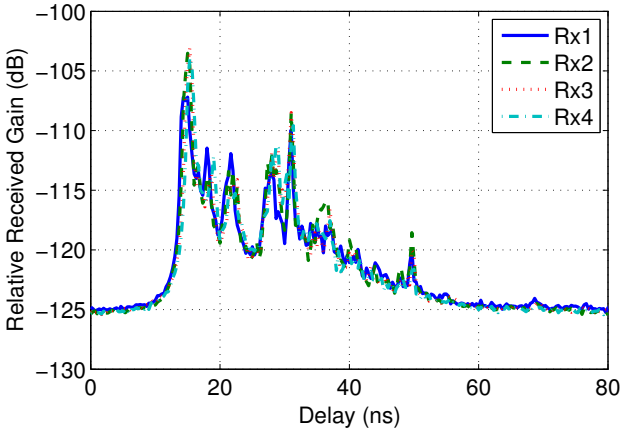


Fig. 3. PDP averaged over all Tx antennas for the 4 Rx users under the FAR scenario.

function (ecdf) of the LOS relative received gain and mean noise level are presented in Fig. 4 for all three scenarios for a given Rx user. An average value of $\approx -125$ dB was

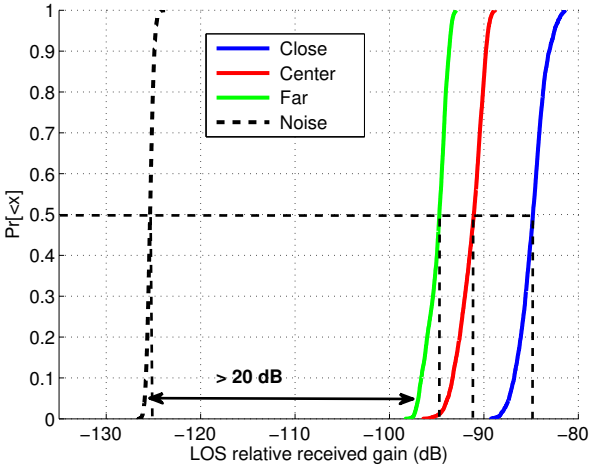


Fig. 4. Ecdf of the LOS received gain for all scenarios and noise.

computed for the noise level from all PDPs. It is concluded from this figure that the difference between the LOS relative gain and mean noise level is always greater than 20 dB for any scenarios. Hence, a 20 dB threshold was selected to compute N. The counting process is illustrated in Fig. 5 for one of the far scenario Tx-Rx link. Also, in order to only identify the peaks considered to contribute to the radio channel, a sliding window analysis was locally applied at each point to avoid the overestimation of N due to the inverse Fourier transform filtering effects. For each delay point, the corresponding relative gain is compared with the one from the previous and next point. The used value for the comparison is 0.8 dB and was empirically obtained from the data.

Figure 6 presents the ecdf of the number of NLOS MPC averaged over all users for the three investigated scenarios and demonstrates the radio channel wealth in terms of scattering

This article has been accepted for publication in a future issue of this journal, but has not been fully edited. Content may change prior to final publication. Citation information: DOI 10.1109/ACCESS.2018.2876225, IEEE Access



components. The distribution and shape of the number of NLOS MPC is clearly dependent on the scenario. For instance, the median value increases from 5-6 to 20 components with the Tx-Rx distance and the values are also more spread. It is observed from the measurements that the decrease of the LOS gain with the Tx-Rx distance is faster than for the NLOS components. Hence, more NLOS MPC appear within the selected threshold. For instance, the ecdf of the NLOS MPC is also presented in Fig. 6. In addition, the number of NLOS MPC are less spread for the close and center scenario compared with the far scenario (between 1 and 14, 5 and 32, 9 and 55 for the close, center, and far scenario, respectively). This effect could be due to a higher order of reflection for the far scenarios thus generating more specular and diffuse components contributing to the channel power and resulting in larger delay spread values.

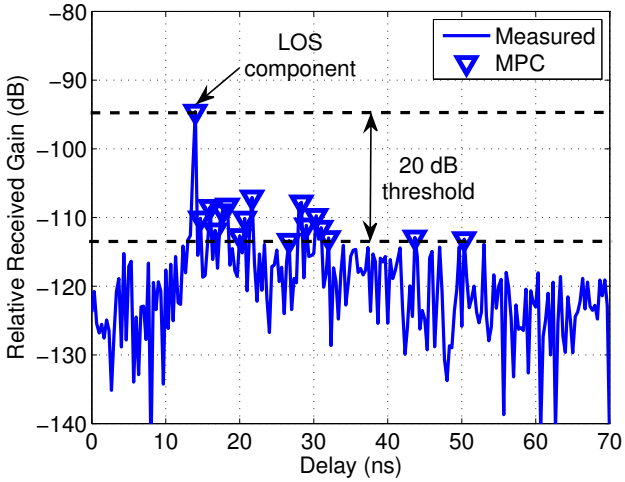


Fig. 5. Example of measured PDP and selected MPC with a 20 dB threshold for the far scenario.

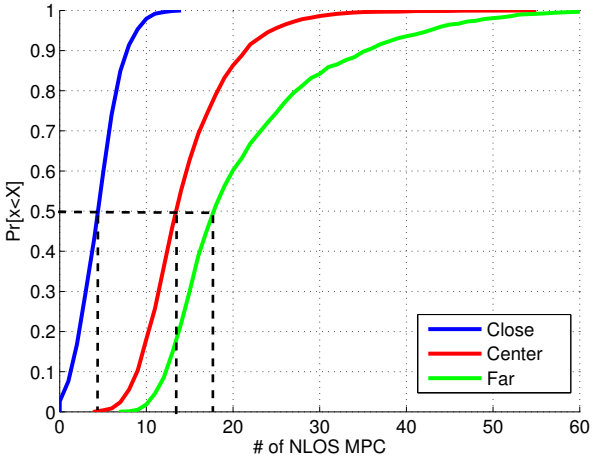


Fig. 6. Number of NLOS MPC averaged over all rx users for all scenarios with a 20 dB threshold.

Figure 7 presents the ecdf of $K$ for the 3 scenarios and for Rx user 3. The number of NLOS MPC was selected from the previous analysis using a 20 dB threshold. Choosing one receiver position does not change the results because all users share similar behaviors on a large scale. The data show that small $K$ values (faded LOS) are obtained for large Tx-Rx distances (center and far) whereas large values (strong LOS) are obtained for the close scenario. For a given scenario, the results indicate spread $K$ values thus highlighting the diversity of the fading mechanisms between each Tx-Rx link. This is particularly true for the close scenario where $K$ values vary between 0 to 20 dB. These results clarify the nature of the massive MIMO radio channel with rich fading characteristics even for a simple LOS condition. This could then be exploited when it comes to the correlation notion.

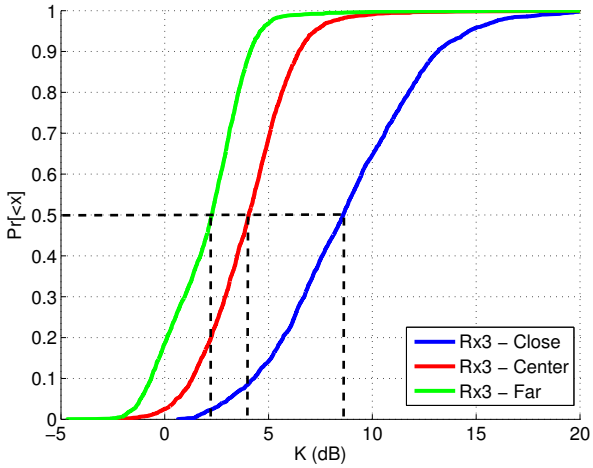


Fig. 7. Ecdf of the Rice factor $K$ (in dB) for all scenarios and Rx user 3 with a 20 dB threshold.

Figure 8(a) shows that $\rho_{ij}^{inter}$ computed for the 3 scenarios all perform nearly like Rayleigh channels; scenario which provides the lowest $\rho_{ij}^{inter}$ bound. Note that the 50×50 URA has been reshaped into a 2500-element row vector to illustrate properly the correlation. Evidently, the larger the number of antennas in the Tx array the more the ideal i.i.d. case can be approached. Nonetheless, very satisfactory results ($\rho_{ij}^{inter} < 0.2$) can be obtained with only 50 antennas ($\sim 7\times7$ URA) and are promising if the deployment massive MIMO is considered in this frequency range or even a lower millimetric band.

Consequently, this shows that the degrees of freedom are offered by the spatial diversity at Tx. This is further investigated by analyzing the intracorrelation characteristics. Figure 8(b) presents the intracorrelation factor $\rho_{km_{ref}}^{intra}$ for the 3 scenarios and Rayleigh channels case. For each scenario, $\rho_{km_{ref}}^{intra}$ is computed with respect to all possible 2500 reference antenna positions. The curves corresponding to the fastest $\rho_{km_{ref}}^{intra}$ decrease (lower bound - LB) and slowest decrease (upper bound - UB) are presented. These two curves illustrate the worst and best case scenario depending on the selected reference antenna. In contrast with $\rho_{ij}^{inter}$, the $\rho_{km_{ref}}^{intra}$ values are larger than for Rayleigh channels as expected due to the heterogeneous nature of the Tx-Rx fading distribution discussed previously. It is observed that the difference between the LB and UB curve decreases as the Tx is moved away

This article has been accepted for publication in a future issue of this journal, but has not been fully edited. Content may change prior to final publication. Citation information: DOI 10.1109/ACCESS.2018.2876225, IEEE Access



from the Rx users. For the close scenario, a strong Rice component has been observed in Fig. 7 which could result in a stronger correlation between the studied user channel vectors. However, the LB curve suggests that the vectors are sufficiently decorrelated by choosing the adequate reference antenna. In other words, different intracorrelation behavior and statistics could be obtained whether the selected antenna experiences small or large $K$ values. For the Far scenario, the LB and UB curves are rather similar due to the dominance of small $K$ values at the level of most reference antennas. It is interesting to mention that the large number of antennas ensures that all curves asymptotically converge towards the Rayleigh channels case. Finally, these results support the fact that strong intracorrelation is not a prerequisite to obtain low intercorrelation values. This is an important finding of this work which enables massive MIMO in this frequency range even under LOS conditions.

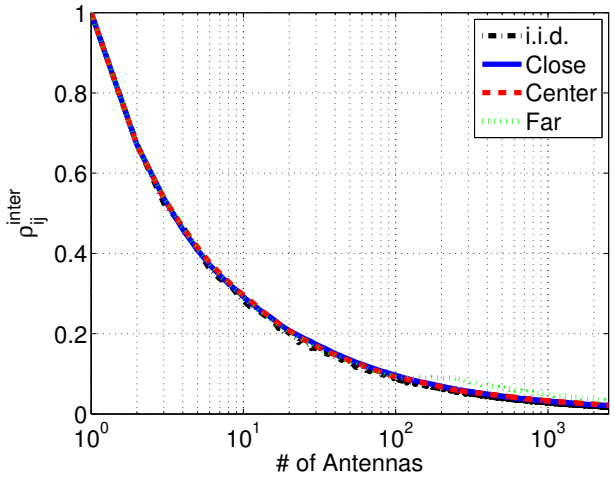


(a)

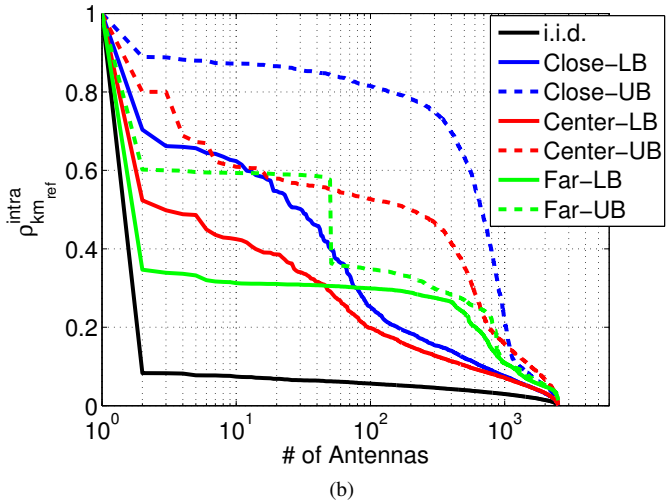


(b)

Fig. 8. (a) Intercorrelation between the 4 users and (b) intracorrelation for user 1. The Rayleigh channel (i.i.d.) curve is plotted for the sake of comparison.

Although the results brought by Fig. 8(b) are interesting for channel modeling purposes, they are not satisfying to understand the intra-intercorrelation relationship and a deeper analysis is required. To this end, the correlation concepts developed in this work were also applied to the phase and module (amplitude). It is expected strong phase variations compared to the amplitude in this frequency range. However, it is rather original to quantitatively investigate their respective contribution to the intercorrelation:

$$h_{kmf} = |h_{kmf}|.e^{j\theta_{kmf}}, \tag{9}$$

where $|h_{kmf}|$ and $\theta_{kmf}$ are the module and phase of the complex massive MIMO transfer function, respectively.

First, Fig. 9 presents the inter- and intracorrelation computed strictly using $|h_{kmf}|$ instead of $h_{kmf}$ in Eqs. (2)-(4) for the studied and Rayleigh channel scenarios. For each scenario, $\rho_{km_{ref}}^{intra}$ is computed with respect to all possible 2500 reference antenna positions and only the curves corresponding to the slowest $\rho_{km_{ref}}^{intra}$ decrease (lower bound - LB) and fastest decrease (upper bound - UB) are shown in Fig. 9(b). Intra- and intercorrelation values greater than 0.8 are obtained indicating that the module does not contribute much to the global intercorrelation (Fig. 8(a)) even for the Rayleigh channel case. In addition, it can be observed that the values computed for the three scenarios are close to the ideal scenario and get closer as Tx is moved away from the users. The latter effect is attributed to the $K$ values which are more distributed resulting in additional decorrelation. These results are in complete contrast with those presented in Fig. 10 from the computation of the intra- and intercorrelation using the phase under the same conditions. For instance, the $\rho_{ij}^{inter}$ values are in excellent agreement with Fig. 8(a) for all studied cases and are attributed to the low $\rho_{km_{ref}}^{intra}$ values (Fig. 8(b)). Hence, it can be safely concluded from this analysis that the low phase intracorrelation values (at Tx side) underlining strong phase variations is the major contributor of the decorrelation between users for the investigated mmW frequency range. It follows the fading distributions are not necessarily the best approach to evaluate the massive MIMO performance on a large-scale since the module contribution, despite the fading diversity, to the intercorrelation is marginal.

### A. Power to interference ratio and Condition number

Here, the condition number $\kappa$ and power to interference ratio $\gamma(\mathbf{G})$ have been computed as a function of the number of increasing activated Tx antennas from 1 to $M = 50 \times 50$. First, Fig. 11 presents the ecdf of $\kappa$ averaged over all users and frequency bins for the investigated scenarios and Rayleigh channel case denoted by i.i.d. in the different figures. The $\kappa$ values are very close to the ideal case for the far and center scenarios but deviate as the Tx is moved closer to Rx. Nonetheless, since most of the $\kappa$ values are close to 1 and less than 1.5, it can be safely assumed that all Rx users are spatially uncorrelated. Evidently, for $\kappa$ values close to 1, the power could be equally distributed among Rx users and same capacity could be reached within the same time-frequency slot. Also, since the interference between users is marginal, the system architecture complexity (notably at the Rx side) could be considerably reduced.

In contrast, for large $\kappa$ values, only a subset of the Rx users receive most of the power as they experience different

This article has been accepted for publication in a future issue of this journal, but has not been fully edited. Content may change prior to final publication. Citation information: DOI 10.1109/ACCESS.2018.2876225, IEEE Access



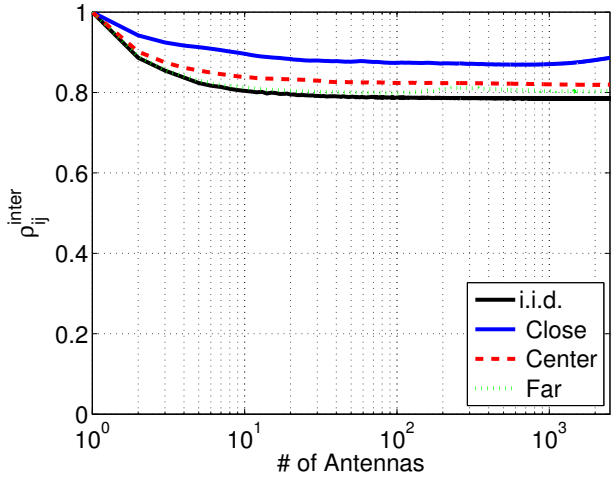


(a)

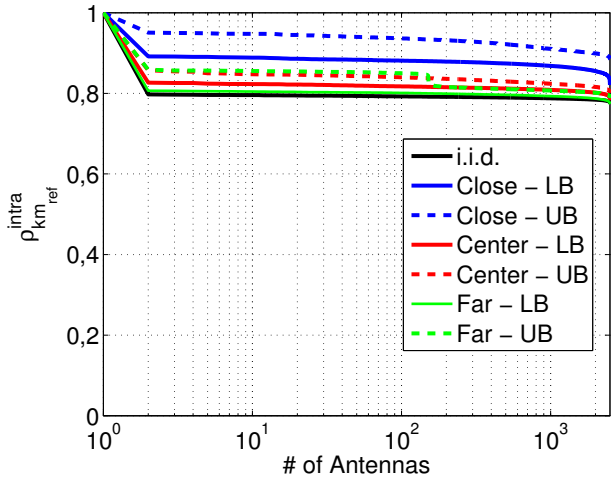


(b)

Fig. 9. (a) Intercorrelation between the 4 users and (b) intracorrelation of the channel vector modules for Rx user 1 computed from $|h_{kmf}|$. The Rayleigh channel curve is plotted for the sake of comparison.

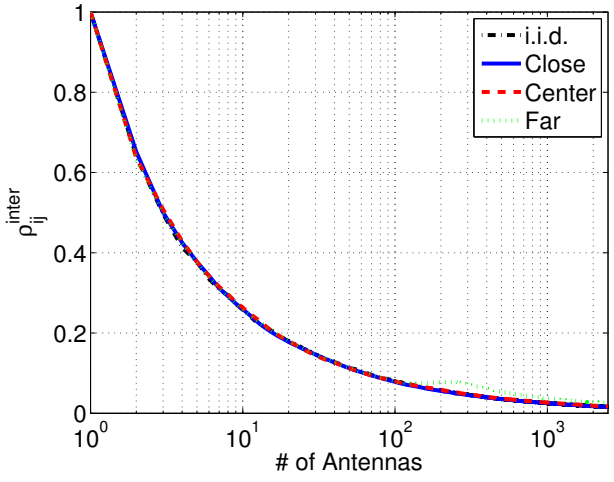


(a)

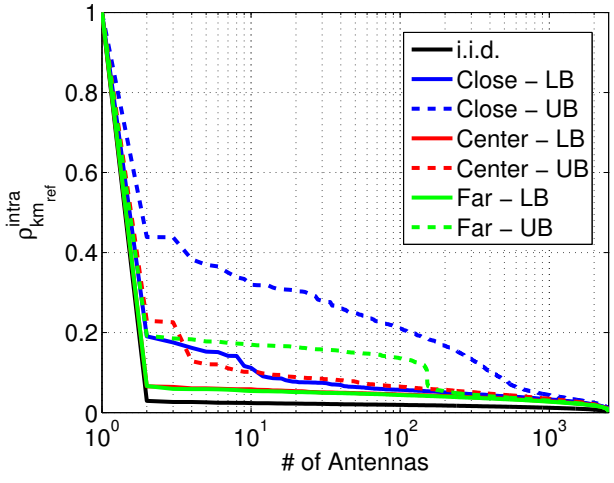


(b)

Fig. 10. (a) Intercorrelation between the 4 users and (b) intracorrelation of the channel vector phases for Rx user 1 computed from $\theta_{kmf}$. The Rayleigh channel curve is plotted for the sake of comparison.

propagation channels and the others interfere with each other. For those cases, the condition number is not enough to quantify the spatial separation between users and the knowledge or partial knowledge of the channel state information (CSI) becomes critical to optimize the capacity allocation among Rx users. Since all $\kappa$ values reported in this work are too small to fall into this category, a thorough discussion on the capacity is outside of the scope of this paper. Here, it could be argued that the condition number is a good macroscopic indicator to describe the overall intercorrelation.

It can be observed that for all scenarios, approximately 90 $\%$ of the condition number values are between 1.1 and 1.5 and only a very small percentage of values is greater than 1.5. These values, even for the Far scenario, illustrate the channel hardening aspect which is a phenomenon that occurs when the number of base stations and number of single-antenna users increase leading to a nearly diagonal correlation matrix. This concept is detailed in [37].

Finally, Fig. 12 presents the power to interference ratio $\gamma(\mathbf{G})$ averaged over all users and frequency points for the investigated scenarios and Rayleigh channel case. For the ideal Rayleigh channel case ($\gamma(\mathbf{G}) \approx 1$), the electromagnetic energy focusing toward each of the Rx users is optimal without any interference from other users (i.e. the signal to interference plus noise ratio (SINR) is maximized). In other words, Rx users are spatially uncorrelated. The results show the excellent behavior of the massive MIMO configuration for the three investigated scenarios with respect to the Rayleigh channel case. It can also be observed that electromagnetic energy focusing is best for the close scenario but still very good for the center and far scenarios. Consequently, these results agree well with those obtained from the intercorrelation and $\kappa$ study for the studied scenarios. However, in comparison with $\kappa$, $\gamma(\mathbf{G})$ provides additional information about the interference between users which could impact the SINR and degrade the system performance. In addition, it can be observed in Fig. 12 for the Close scenario that the curve is very close to the Rayleigh channel (i.i.d.) case. For the Center and Far scenario, more

than 95% of the values are close to 1. This results confirms the previous observation on the condition number proving that the mmW channel provides limited interference between users.

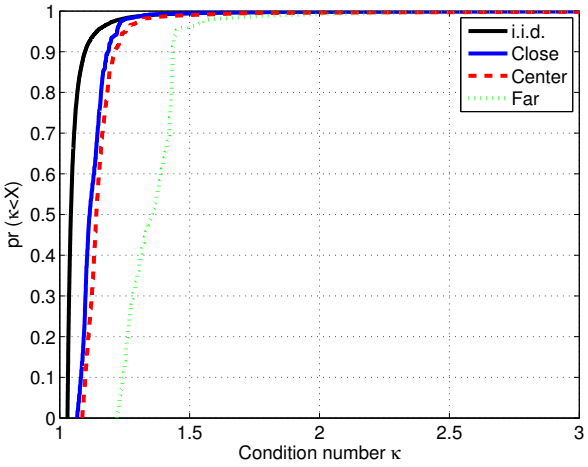


Fig. 11. Ecdf of the condition number $\kappa$ averaged over all Rx users and frequency bins for the three scenarios and Rayleigh channel case.

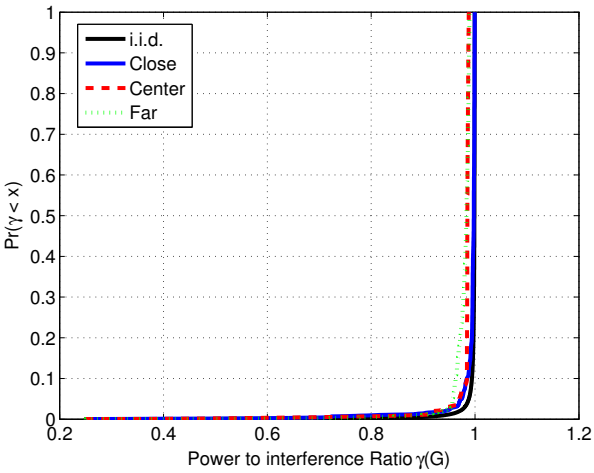


Fig. 12. Ecdf of the power to interference ratio $\gamma(\mathbf{G})$ averaged over all Rx users frequency bins for the three scenarios and Rayleigh channel case.

Table II presents a summary of the intercorrelation and LB/UB intracorrelation metric values obtained for a $50 \times 50$, $25 \times 25$, $12 \times 12$ and $7 \times 7$ array and for all investigated scenarios as well as the reference Rayleigh channel case. The phase and module correlation values are also included to highlight the phase decorrelation processes. This table clearly shows the many benefits of the application of massive MIMO in mmW frequency bands even with small arrays.

## V. Conclusion

In this work, realistic massive MIMO measurements were performed at 94 GHz over a 3 GHz bandwidth with a large $50 \times 50$ URA for Tx and a 4-element ULA for Rx under three different LOS scenarios. Most of the mmW massive MIMO system advantages can be provided in the investigated scenarios despite the strong Rice propagation characteristics. The number of NLOS MPC contributing to the radio channel as well as the Ricean K-factor have been characterized and demonstrate the complexity of the fading properties between the Tx array and Rx users.

The intracorrelation describing the correlation between channel vectors for a given user have been introduced. This notion is a preliminary effort to understand the mechanisms responsible of the spatial decorrelation between Rx users. This orthogonality is assessed in this work by a discussion on the intercorrelation, condition number, or even power to interference ratio.

The results demonstrate without ambiguity the capability of massive MIMO systems in this frequency range to reach orthogonal Tx-Rx streams even for a reduced massive array subset in a Rician environment. In our case, a $7\times7$ compact array of $\sim 6$ cm $\times$ 6 cm ($\sim 21\lambda \times 21\lambda$) is sufficient to obtain intercorrelation values well below 0.2 meaning very good spatial separation of the 4 users. Furthermore, it is shown that the channel phase variation at Tx side is the main contributor of the decorrelation between users. This result must be further investigated to deepen the comprehension of the decorrelation mechanisms in different frequency bands. Finally, the notion of intracorrelation and its dependence on the reference antenna element was observed as an important indicator for antenna allocation strategies and precoding schemes in the context of massive MIMO.

## Acknowledgement

This work was funded through a Short Term Scientific Mission (STSM) by the IRACON COST Action CA15104 under the grant COST-STSM-ECOST-STSM-CA15104-300516-077981 and MINECO, Spain under the grant TEC2016-78028-C3-P. It was also supported through the OS4 SMARTIES research program by the ELSAT2020 project co-financed by the European Union with the European Regional Development Fund, the French state, and the Hauts-de-France Region Council.

## References

[1] *CISCO Global Cloud Index (GCI).* [Online]. Available: http://www.cisco.com/c/dam/en/us/solutions/collateral/service-provider/global-cloud-index-gci/white-paper-c11-738085.pdf

[2] T. Rappaport, *Wireless Communications: Principles and Practice*, 2nd ed. Upper Saddle River, NJ, USA: Prentice Hall PTR, 2001.

[3] S. Salous, V. D. Esposti, F. Fuschini, R. S. Thomae, R. Mueller, D. Dupleich, K. Haneda, J. M. M. Garcia-Pardo, J. P. Garcia, D. P. Gaillot, S. Hur, and M. Nekovee, "Millimeter-wave propagation: Characterization and modeling toward fifth-generation systems. [wireless corner]," *IEEE Antennas and Propagation Magazine*, vol. 58, no. 6, pp. 115–127, Dec 2016.

TABLE II
CORRELATION PARAMETERS OF MASSIVE MIMO CHANNEL

| Array size | Scenario | Intercorrelation | | | LB/UB Intracorrelation | | |
|---|---|---|---|---|---|---|---|
| | | Total | Phase | Module | Total | Phase | Module |
| $50 \times 50$ | Close | 0.02 | 0.016 | 0.88 | 0.003/0.005 | 0.0021/0.0022 | 0.83/0.89 |
| | Center | 0.02 | 0.017 | 0.82 | 0.004/0.005 | 0.0010/0.0012 | 0.78/0.80 |
| | Far | 0.04 | 0.02 | 0.80 | 0.002/0.004 | 0.017/0.017 | 0.77/0.79 |
| | Rayleigh | 0.01 | 0.0007 | 0.77 | 0.011 | 0.012 | 0.76 |
| $25 \times 25$ | Close | 0.04 | 0.03 | 0.86 | 0.04/0.06 | 0.10/0.54 | 0.87/0.92 |
| | Center | 0.04 | 0.03 | 0.81 | 0.03/0.04 | 0.81 | 0.09/0.27/0.83 |
| | Far | 0.06 | 0.04 | 0.80 | 0.03/0.04 | 0.19/0.25 | 0.80/0.81 |
| | Rayleigh | 0.03 | 0.04 | 0.78 | 0.014 | 0.03 | 0.77 |
| $12 \times 12$ | Close | 0.08 | 0.06 | 0.87 | 0.05/0.19 | 0.20/0.80 | 0.88/0.93 |
| | Center | 0.09 | 0.06 | 0.82 | 0.06/0.04 | 0.17/0.51 | 0.82/0.84 |
| | Far | 0.08 | 0.07 | 0.80 | 0.04/0.12 | 0.29/0.34 | 0.80/0.85 |
| | Rayleigh | 0.07 | 0.05 | 0.78 | 0.018 | 0.06 | 0.77 |
| $7 \times 7$ | Close | 0.14 | 0.11 | 0.88 | 0.06/0.24 | 0.40/0.84 | 0.88/0.94 |
| | Center | 0.13 | 0.11 | 0.82 | 0.05/0.07 | 0.29/0.55 | 0.82/0.84 |
| | Far | 0.13 | 0.11 | 0.8 | 0.04/0.15 | 0.30/0.57 | 0.80/0.85 |
| | Rayleigh | 0.12 | 0.06 | 0.78 | 0.02 | 0.11 | 0.77 |


[4] *The 5G Infrastructure Public Private Partnership*, http://5g-ppp.eu/.

[5] M. Tercero, P. von Wrycza, A. Amah, J. Widmer, M. Fresia, V. Frascolla, J. Lorca, T. Svensson, M. H. Hamon, S. D. Roblot, A. Vijay, M. Peter, V. Sgardoni, M. Hunukumbure, J. Luo, and N. Vucic, "5g systems: The mmmagic project perspective on use cases and challenges between 6 -100 ghz," in *2016 IEEE Wireless Communications and Networking Conference*, April 2016, pp. 1–6.

[6] L. Jofre, J. Romeu, S. Capdevila, J. Abril, E. Nova, and M. Alonso, "The "challenging"world of terahertz radiation and imaging," in *Proceedings of the 5th European Conference on Antennas and Propagation (EUCAP)*, April 2011, pp. 3470–3475.

[7] S. D'Amico, M. De Matteis, O. Rousseaux, K. Philips, B. Gyselinck, D. Neirynck, and A. Baschirotto, *Ultra Wide Band in Medical Applications*. Berlin, Heidelberg: Springer Berlin Heidelberg, 2010, pp. 43–60. [Online]. Available: https://doi.org/10.1007/978-3-642-05167-8_4

[8] A. P. G. Ariza, R. Müller, F. Wollenschläger, A. Schulz, M. Elkhouly, Y. Sun, S. Glisic, U. Trautwein, R. Stephan, J. Müller, R. S. Thomä, and M. Hein, "60 ghz ultrawideband polarimetric mimo sensing for wireless multigigabit and radar," *IEEE Transactions on Antennas and Propagation*, vol. 61, no. 4, pp. 1631–1641, April 2013.

[9] *Applications and use cases of millimetre wave transmission*. [Online]. Available: http://www.etsi.org/deliver/etsi_gs/mWT/001_099/002/01.01.01_60/gs_mWT002v010101p.pdf

[10] T. L. Marzetta, "Noncooperative cellular wireless with unlimited numbers of base station antennas," *IEEE Transactions on Wireless Communications*, vol. 9, no. 11, pp. 3590–3600, November 2010.

[11] X. Gao, O. Edfors, F. Rusek, and F. Tufvesson, "Linear pre-coding performance in measured very-large mimo channels," in *Vehicular Technology Conference (VTC Fall), 2011 IEEE*, Sept 2011, pp. 1–5.

[12] F. Rusek, D. Persson, B. K. Lau, E. G. Larsson, T. L. Marzetta, O. Edfors, and F. Tufvesson, "Scaling up mimo: Opportunities and challenges with very large arrays," *IEEE Signal Processing Magazine*, vol. 30, no. 1, pp. 40–60, Jan 2013.

[13] L. Lu, G. Y. Li, A. L. Swindlehurst, A. Ashikhmin, and R. Zhang, "An overview of massive mimo: Benefits and challenges," *IEEE Journal of Selected Topics in Signal Processing*, vol. 8, no. 5, pp. 742–758, Oct 2014.

[14] E. G. Larsson, O. Edfors, F. Tufvesson, and T. L. Marzetta, "Massive mimo for next generation wireless systems," *IEEE Communications Magazine*, vol. 52, no. 2, pp. 186–195, February 2014.

[15] S. Malkowsky, J. Vieira, L. Liu, P. Harris, K. Nieman, N. Kundargi, I. C. Wong, F. Tufvesson, V. Owall, and O. Edfors, "The world's first real-time testbed for massive mimo: Design, implementation, and validation," *IEEE Access*, vol. 5, pp. 9073–9088, 2017.

[16] P. Harris, W. B. Hasan, S. Malkowsky, J. Vieira, S. Zhang, M. Beach, L. Liu, E. Mellios, A. Nix, S. Armour, A. Doufexi, K. Nieman, and N. Kundargi, "Serving 22 users in real-time with a 128-antenna massive mimo testbed," in *2016 IEEE International Workshop on Signal Processing Systems (SiPS)*, Oct 2016, pp. 266–272.

[17] C. Shepard, H. Yu, N. Anand, E. Li, T. Marzetta, R. Yang, and L. Zhong, "Argos: Practical many-antenna base stations," in *Proceedings of the 18th Annual International Conference on Mobile Computing*

*and Networking*, ser. Mobicom '12. New York, NY, USA: ACM, 2012, pp. 53–64. [Online]. Available: http://doi.acm.org/10.1145/2348543.2348553

[18] *TitanMIMO*, https://www.nutaq.com/5g-massive-mimo-testbed.

[19] *Samsung and Sprint Conduct Real-World Massive MIMO Testing at Mobile World Congress Fall 2017*, https://insights.samsung.com/2017/09/11/samsung-and-sprint-conduct-real-world-massive-mimo-testing-at-mobile-world-congress-fall-2017/.

[20] A. L. Swindlehurst, E. Ayanoglu, P. Heydari, and F. Capolino, "Millimeter-wave massive mimo: the next wireless revolution?" *IEEE Communications Magazine*, vol. 52, no. 9, pp. 56–62, September 2014.

[21] F. Boccardi, R. W. Heath, A. Lozano, T. L. Marzetta, and P. Popovski, "Five disruptive technology directions for 5g," *IEEE Communications Magazine*, vol. 52, no. 2, pp. 74–80, February 2014.

[22] F. Al-Ogaili and R. M. Shubair, "Millimeter-wave mobile communications for 5g: Challenges and opportunities," in *2016 IEEE International Symposium on Antennas and Propagation (APSURSI)*, June 2016, pp. 1003–1004.

[23] T. S. Rappaport, S. Sun, R. Mayzus, H. Zhao, Y. Azar, K. Wang, G. N. Wong, J. K. Schulz, M. Samimi, and F. Gutierrez, "Millimeter wave mobile communications for 5g cellular: It will work!" *IEEE Access*, vol. 1, pp. 335–349, 2013.

[24] S. A. Busari, K. M. S. Huq, S. Mumtaz, L. Dai, and J. Rodriguez, "Millimeter-wave massive mimo communication for future wireless systems: A survey," *IEEE Communications Surveys Tutorials*, vol. PP, no. 99, pp. 1–1, 2017.

[25] S. Kirthiga and M. Jayakumar, "Performance studies and review of millimeter wave mimo beamforming at 60 ghz," *Procedia Technology*, vol. 21, pp. 658 – 666, 2015. [Online]. Available: http://www.sciencedirect.com/science/article/pii/S2212017315003072

[26] T. E. Bogale and L. B. Le, "Massive mimo and mmwave for 5g wireless hetnet: Potential benefits and challenges," *IEEE Vehicular Technology Magazine*, vol. 11, no. 1, pp. 64–75, March 2016.

[27] J. Huang, C. X. Wang, R. Feng, J. Sun, W. Zhang, and Y. Yang, "Multi-frequency mmwave massive mimo channel measurements and characterization for 5g wireless communication systems," *IEEE Journal on Selected Areas in Communications*, vol. 35, no. 7, pp. 1591–1605, July 2017.

[28] A. Taira, H. Iura, K. Nakagawa, S. Uchida, K. Ishioka, A. Okazaki, S. Suyama, T. Obara, Y. Okumura, and A. Okamura, "Performance evaluation of 44ghz band massive mimo based on channel measurement," in *2015 IEEE Globecom Workshops (GC Wkshps)*, Dec 2015, pp. 1–6.

[29] J. Chen, X. Yin, and S. Wang, "Measurement-based massive mimo channel modeling in 13-17 ghz for indoor hall scenarios," in *2016 IEEE International Conference on Communications (ICC)*, May 2016, pp. 1–5.

[30] M. T. Martinez-Ingles, J. M. M. Garcia-Pardo, D. P. Gaillot, J. Pascual-Garcia, J. V. Rodriguez, L. J. Llácer, and M. Lienard, "Polarimetric indoor measurements at 94 ghz," in *2016 10th European Conference on Antennas and Propagation (EuCAP)*, April 2016, pp. 1–3.

[31] F. Kaltenberger, D. Gesbert, R. Knopp, and M. Kountouris, "Correlation and capacity of measured multi-user mimo channels," in *2008 IEEE 19th International Symposium on Personal, Indoor and Mobile Radio Communications*, Sept 2008, pp. 1–5.

[32] D. Löschenbrand, M. Hofer, and T. Zemen, "Ray-tracer based channel characteristics for distributed massive mimo," *European Cooperation in Science and Technology EURO-COST Lisbon, Portugal*, 2017.

[33] http://www.miwv.com/.

[34] http://www.arrickrobotics.com/.

[35] J. A. Fessler and A. O. Hero, "Space-alternating generalized expectation-maximization algorithm," *Signal Processing, IEEE Transactions on*, vol. 42, no. 10, pp. 2664–2677, 1994.

[36] A. Richter, "Estimation of radio channel parameters: Models and algorithms," Ph.D. dissertation, Technische Universität Ilmenau, Fakültat für Elektrotechnik und Informationstechnik, Ilmenau, DE, 2005. [Online]. Available: http://www.db-thueringen.de/servlets/DerivateServlet/Derivate-7407/ilm1-2005000111.pdf

[37] T. L. Narasimhan and A. Chockalingam, "Channel hardening-exploiting message passing (chemp) receiver in large mimo systems," in *2014 IEEE Wireless Communications and Networking Conference (WCNC)*, April 2014, pp. 815–820.